

行政院國家科學委員會專題研究計畫 期末報告

不均勻外力作用於層狀半空間內之解析解

計畫類別：個別型
計畫編號：NSC 101-2221-E-009-172-
執行期間：101年08月01日至102年09月30日
執行單位：國立交通大學土木工程學系（所）

計畫主持人：劉俊秀

計畫參與人員：此計畫無其他參與人員

報告附件：出席國際會議研究心得報告及發表論文

公開資訊：本計畫可公開查詢

中華民國 102年12月29日

中文摘要：本研究主要是要求得埋在層狀半空間中任意分佈外力所造成之地盤反應。目前能夠將外力加在層狀半空間內部的解，一般是指 Green Function 的解，但 Green Function 為一集中載重之解，因此會有奇異點(singularity)之現象。而本文是以任意分佈載重模擬外力，因此不會有奇異點的現象。這對目前利用邊界元素法(BEM)求地盤振動與基礎阻抗矩陣將會有大幅度之改進。

本研究之求解過程中，將假設外力在徑向(r-方向)之分佈為片段線性(piecewise linear)，在 θ -方向可分解成傅立葉級數(Fourier Series)。此分佈外力可作用在任何深度。然後可利用主持人過去所發展之方法直接求圓柱座標系統中之波動方程式之解，其最後之解將為一 Bessel Function 之積分式。本文法最大之特點為外力作用位置之位移沒有奇異的現象。

又由於載重片段線性，因此只要求得一小區域線性分析之解，即可求得所有片段線性分佈之解。本研究將漸漸縮小分佈載重面積，以觀察其應力的集中性，及其對位移的影響。

中文關鍵詞：Wave Propagation, Analytic Solution, Green Function

英文摘要：The paper is to deal with the problem of the response of stratified half-space subjected to an arbitrary distributed loading on an axial symmetric area buried in stratified half-space. Except boundary element method, the response to a force buried in a stratified half-space is rarely dealt with. However, Green function employed in boundary element method will creat singularity situation at the location of source point. The presented method can avoid the singularity situation, since the external loading is not a concentrated load and is arbitrarily distributed over an axial symmetric area buried in stratified half-space.

In the process of the solution, the arbitrarily distributed loading can be decomposed into a Fourier Series in θ -direction and piecewise linear distribution in r-direction is assumed for each Fourier component. Then the wave equations in cylindrical coordinates are directly solved using the technique developed by the author. The solution will be an integral of Bessel function with respect to

wave number. The advantage of the method will be that singularity problem can be avoided.

Since the distributed loading is piecewise linear, one just need to solve the problem for a triangular distribution on an axial symmetric area and then sums up all the solution for all the triangular distribution .This summation will be the solution for arbitrary distributed loading. Some numerical results for shrinking the distributed area will be given to show the concentrated effect of the distributed loading.

英文關鍵詞： Wave Propagation, Analytic Solution, Green Function

行政院國家科學委員會補助專題研究計畫成果報告

(期中進度報告/期末報告)

不均勻外力作用於層狀半空間內之解析解

計畫類別：個別型計畫 整合型計畫

計畫編號：NSC 101-2221-E-009-172

執行期間：101年8月1日至102年9月30日

執行機構及系所：國立交通大學土木工程學系(所)

計畫主持人：劉俊秀

共同主持人：

計畫參與人員：

本計畫除繳交成果報告外，另含下列出國報告，共 1 份：

執行國際合作與移地研究心得報告

出席國際學術會議心得報告

期末報告處理方式：

1. 公開方式：

非列管計畫亦不具下列情形，立即公開查詢

涉及專利或其他智慧財產權，一年二年後可公開查詢

2. 「本研究」是否已有嚴重損及公共利益之發現：否 是

3. 「本報告」是否建議提供政府單位施政參考 否 是， (請列舉提供之單位；本會不經審議，依勾選逕予轉送)

中 華 民 國 102 年 12 月 29 日

國科會補助專題研究計畫成果報告自評表

請就研究內容與原計畫相符程度、達成預期目標情況、研究成果之學術或應用價值（簡要敘述成果所代表之意義、價值、影響或進一步發展之可能性）、是否適合在學術期刊發表或申請專利、主要發現（簡要敘述成果是否有嚴重損及公共利益之發現）或其他有關價值等，作一綜合評估。

1. 請就研究內容與原計畫相符程度、達成預期目標情況作一綜合評估

達成目標

未達成目標（請說明，以 100 字為限）

實驗失敗

因故實驗中斷

其他原因

說明：

2. 研究成果在學術期刊發表或申請專利等情形：

論文： 已發表 未發表之文稿 撰寫中 無

專利： 已獲得 申請中 無

技轉： 已技轉 洽談中 無

其他：（以 100 字為限）

投稿 Journal of Earthquake Engineering and Structure Dynamic

3. 請依學術成就、技術創新、社會影響等方面，評估研究成果之學術或應用價值（簡要敘述成果所代表之意義、價值、影響或進一步發展之可能性），如已有嚴重損及公共利益之發現，請簡述可能損及之相關程度（以 500 字為限）

本研究主要突破為求得小面積內分佈載重之解析解,與 Green function 相較,本研究之解沒有奇異(singularity)值問題。

中文摘要。

關鍵詞: Wave Propagation, Analytic Solution, Green Function

本研究主要是要求得埋在層狀半空間中任意分佈外力所造成之地盤反應。目前能夠將外力加在層狀半空間內部的解，一般是指Green Function的解，但Green Function 為一集中載重之解，因此會有奇異點(singularity)之現象。而本文是以任意分佈載重模擬外力，因此不會有奇異點的現象。這對目前利用邊界元素法(BEM)求地盤振動與基礎阻抗矩陣將會有大幅度之改進。

本研究之求解過程中，將假設外力在徑向(r-方向)之分佈為片段線性(piecewise linear)，在 θ -方向可分解成傅立葉級數(Fourier Series)。此分佈外力可作用在任何深度。然後可利用主持人過去所發展之方法直接求圓柱座標系統中之波動方程式之解，其最後之解將為一Bessel Function 之積分式。本文法最大之特點為外力作用位置之位移沒有奇異的現象。

又由於載重片段線性，因此只要求得一小區域線性分析之解，即可求得所有片段線性分佈之解。本研究將漸漸縮小分佈載重面積，以觀察其應力的集中性，及其對位移的影響。

Abstract

Keyword: Wave Propagation, Analytic Solution, Green Function

The paper is to deal with the problem of the response of stratified half-space subjected to an arbitrary distributed loading on an axial symmetric area buried in stratified half-space. Except boundary element method, the response to a force buried in a stratified half-space is rarely dealt with. However, Green function employed in boundary element method will create singularity situation at the location of source point. The presented method can avoid the singularity situation, since the external loading is not a concentrated load and is arbitrarily distributed over an axial symmetric area buried in stratified half-space.

In the process of the solution, the arbitrarily distributed loading can be decomposed into a Fourier Series in θ -direction and piecewise linear distribution in r -direction is assumed for each Fourier component. Then the wave equations in cylindrical coordinates are directly solved using the technique developed by the author. The solution will be an integral of Bessel function with respect to wave number. The advantage of the method will be that singularity problem can be avoided.

Since the distributed loading is piecewise linear, one just need to solve the problem for a triangular distribution on an axial symmetric area and then sums up all the solution for all the triangular distribution. This summation will be the solution for arbitrary distributed loading. Some numerical results for shrinking the distributed area will be given to show the concentrated effect of the distributed loading.

Introduction

Ground vibration due to near-by sources has been paid attention to over past several decades. Especially, for the sensitive facility and high-tech productions equipment, this vibrations is annoying. Therefore, how to predict the vibrations become an important subject. Wood and Jedele [1] have collected some observed data and deduced them into a simple formula expressing attenuation phenomenon of ground vibrations in term of soil damping and distance between source and observation locations. From more theoretical aspects, Sheng et al. [2] and Krylou [3] have employed Euler beam theory to model whole track including sleepers and ballast and then to solve the problem of moving train. Kaynia et al.[4] have proposed a more sophisticated analysis model, which takes dynamic interaction into account, to evaluate ground vibration induced by passing trains. Moreover, Karlstrom [5] has employed a refined semi-analytic model to investigate the effect on ground vibration due to accelerating train.

Most of the above analysis model, finite element or boundary element methods are used to model half-space medium or layered half-space medium. Regarding analytical approach to evaluate ground vibration due to a specific source, Apsel and Ruco [6] have calculated the vibrations at the locations on half-space medium due to a point source (Green's Function). Vostroukhov [7] et al. have employed integral transform method to obtain ground vibration in layered half-space due to a buried uniform load at a circular area.

Also, Kausel and Peer [8] has employ layer elements to obtain Green function for layered medium. Green function has been the fundamental solution for the boundary element method. However, the singularity situation occurs at the location of source point. The major task of boundary element method is to deal with the singularity problem. The paper is trying to obtain the solution for distributing the point (concentrated) load to a small area. Therefore, the singularity problem will disappears.

In the solution process, the distributed loading on an axial symmetric area can be decomposed into an infinite series of Fourier components with respect to azimuth. For each Fourier components, triangular distribution in r -direction is assumed.

To solve the problem mathematically, the whole layered half-space medium is divided into two domains (upper and lower domains), the upper domain is the domain above the level where the external loading is applied, and the other one is the lower domains which is below the level. For each domain, the technique of decomposing the loading, which is developed by Liou [9], is employed. The decomposed loading will automatically match the forms of boundary values of general solutions of three dimensional wave equations in cylindrical coordinates for the layered stratum. Then,

the boundary conditions of free surface , attenuation phenomenon, and the continuity conditions of displacement and stress components at the interface of the two domains (above and below the level) are imposed to obtain the solution .

The analytical expression for vibration at a specific location in a layered medium will end up with a form of semi-infinite intergration with respect to wave number k , and Rayleigh singular pole existing in the integration path if there is no material damping in the medium. However, if material damping is always assigned in the medium, the singular pole will move away from intergration path. And, from the decaying nature of the integrand with respect to wave number k as proven in Liou's work [10], the vibration can be calculated by integration only up to a certain upper limit k_u without losing accuracy.

The numerical results for the cases of equal magnitude of total loading with different distribution areas will be compared each other. This will show the phenomenon of variation of stress and displacement components around the different distribution areas of the total loading. The solution should be close to Green function solution as the distribution area getting smaller. However, no singularity situation like that in Green function solution at source point will occur in the presented solution.

Analytical Solutions For Dynamic Loadings In Layered Medium

The general solution of the differential equations for wave propagation in cylindrical coordinates is independently found for each layer in layered medium. The displacement and stress continuity conditions at the horizontal interfaces in layered system are then imposed for further expressing the displacement and stress fields in terms of the prescribed dynamic loadings. The total system of prescribed dynamic loadings applied in layered half-space is shown in Figs.1. In Fig.1(a), the shaded area is the locations where dynamic loading is applied. Fig.1(b) shows the distribution of the dynamic load in r-direction for each Fourier component. The prescribed dynamic loadings on axially symmetric area can be expressed in cylindrical coordinates in terms of Fourier components with respect to azimuth as follows :

$$\begin{bmatrix} \bar{\tau}_{rz}(r, \theta) \\ \bar{\sigma}_{zz}(r, \theta) \\ \bar{\tau}_{\theta z}(r, \theta) \end{bmatrix} e^{i\omega t} = \sum_{n=0}^{\infty} \begin{bmatrix} \bar{\tau}_{rz}^n(r) \begin{Bmatrix} \cos(n\theta) \\ \sin(n\theta) \end{Bmatrix} \\ \bar{\sigma}_{zz}^n(r) \begin{Bmatrix} \cos(n\theta) \\ \sin(n\theta) \end{Bmatrix} \\ \bar{\tau}_{\theta z}^n(r) \begin{Bmatrix} \cos(n\theta) \\ \sin(n\theta) \end{Bmatrix} \end{bmatrix} e^{i\omega t} \quad r_1 \leq r \leq r_2, z = h_i \quad (1)$$

where superscript n denotes n^{th} Fourier component in the series; ω is frequency ;

$$r_1 - r_2 = 2\varepsilon .$$

Since the time variation $e^{i\omega t}$ appears on both sides of the equation, it will be omitted hereinafter. For the cases of dynamic loadings applied at arbitrary area, the loading can be expressed by the summation of several axial symmetric areas in Eq.(1) .

Since the external load is applied at level i in Fig1(a), the domain is divided into two domains. One is the domain above level i and the other is the domain below level i . One can consider the domain below level i first. As show in Fig.1(a), the general differential equations for wave propagation in a particular layer j with harmonic excitation can be obtained using the technique separating the dilatational wave from the rotational wave . And the technique of separation of variables is employed to solve the independent differential equations for the dilatational wave and the rotational wave. After combining the solutions for the dilatational and the rotational waves, the general solution of the differential equations of wave propagation for n^{th} Fourier component can be expressed in the matrix form as follows :

$$\begin{cases} u_r(r, z) \begin{pmatrix} \cos n\theta \\ \sin n\theta \end{pmatrix} \\ u_z(r, z) \begin{pmatrix} \cos n\theta \\ \sin n\theta \end{pmatrix} \\ u_\theta(r, z) \begin{pmatrix} -\sin n\theta \\ \cos n\theta \end{pmatrix} \end{cases} = \begin{bmatrix} \begin{pmatrix} \cos n\theta \\ \sin n\theta \end{pmatrix} & 0 & 0 \\ 0 & \begin{pmatrix} \cos n\theta \\ \sin n\theta \end{pmatrix} & 0 \\ 0 & 0 & \begin{pmatrix} -\sin n\theta \\ \cos n\theta \end{pmatrix} \end{bmatrix} \mathbf{J} \boldsymbol{\kappa}_1 \mathbf{e} \mathbf{A} \quad (2)$$

or

$$\mathbf{L} \mathbf{u} = \mathbf{L} \mathbf{J} \boldsymbol{\kappa}_1 \mathbf{e} \mathbf{A}$$

where

$$\mathbf{J} = \begin{bmatrix} J'_n(kr) & 0 & (n/r)J_n(kr) \\ 0 & kJ_n(kr) & 0 \\ (n/r)J_n(kr) & 0 & J'_n(kr) \end{bmatrix} \quad (3)$$

matrix $\boldsymbol{\kappa}_1$ is defined by Eq. (A-1) in Appendix,

vector $\mathbf{A} = (A_1, B_1, C_1, A_2, B_2, C_2)^T$ is unknown coefficient vector determined

from the boundary conditions at the upper and the lower interfaces of the layer, 6×6

diagonal matrix $\mathbf{e} = \text{diag}(e^{-v_j z}, e^{-v'_j z}, e^{-v'_j z}, e^{v_j z}, e^{v'_j z}, e^{v'_j z})$,

$$v_j = \sqrt{k^2 - (\omega^2/c_{pj}^2)}, \quad v'_j = \sqrt{k^2 - (\omega^2/c_{gj}^2)},$$

c_{pj} and c_{gj} are compressional and shear wave velocities respectively in the layer

(j^{th} layer), k is wave number in horizontal direction, $J_n(kr)$ is first kind of Bessel function of order n , and $J'_n(kr) = [dJ_n(kr)/dr]$.

The stress field in the layer can be obtained by differentiating the displacement field of Eq.(2) with respect to the corresponding variables r , z and θ , and then multiplying it with constitutive matrix of elasticity. The stress components on horizontal plane, with the azimuthal variation of matrix L (representing symmetric and antisymmetric Fourier components with respect to $\theta=0$) in Eq.(2) factored out, can then be expressed as follows :

$$t = \begin{Bmatrix} \tau_{rz}(r, z) \\ \sigma_{zz}(r, z) \\ \tau_{\theta z}(r, z) \end{Bmatrix} = \mathbf{J}\boldsymbol{\kappa}_2 \mathbf{eA} \quad (4)$$

where matrix $\boldsymbol{\kappa}_2$ is defined by Eq.(A-2) in Appendix.

Since the unknown coefficients in vector \mathbf{A} are determined from the boundary conditions of the layer, the displacement and the stress fields of Eqs.(2) and (4) can be expressed in terms of the unknown displacement and stress components at the lower interface of the layer [9,11]. Moreover, the displacement and stress components at the upper interface can be combined together and written in terms of the displacement and stress components at the lower interface as follows [9,11]:

$$\mathbf{Y}_{j-1} = \mathbf{Ea}_j \mathbf{E}^{-1} \mathbf{Y}_j \quad (5)$$

where 6×6 matrix $\mathbf{E} = \text{diag}(\mathbf{J}, \mathbf{J})$ in which Bessel matrix \mathbf{J} is shown in Eq.(3),

transfer matrix $\mathbf{a}_j = \boldsymbol{\kappa}^{-1}(d_j) \boldsymbol{\kappa}^{-1}$ is defined by Eq.(A-3) in Appendix in which matrix

$\boldsymbol{\kappa} = \begin{bmatrix} \boldsymbol{\kappa}_1^T & \boldsymbol{\kappa}_2^T \end{bmatrix}^T$, diagonal matrix $\mathbf{e}(d_j) = \mathbf{e}|_{z=d_j}$ in which d_j is the thickness of the

layer, and \mathbf{Y}_{j-1} and \mathbf{Y}_j are the unknown displacement-stress vectors at the upper and the lower interfaces of the layer, respectively.

Consider the total lower domain shown in Fig.1. For a given layer in the system, Eq.(5) shows that the displacement-stress vector at the upper interface can be

expressed in terms of the displacement –stress vector at the lower interface. Therefore, by imposing the displacement and stress continuity conditions at the horizontal interfaces from the first top layer down to the half-space layer, one can obtain the displacement-stress vector at the surface of the total system in terms of the displacement-stress vector at the surface of the half-space layer as expressed by Eq.(6).

$$\mathbf{Y}_i = \mathbf{E} \mathbf{a}_{i+1} \mathbf{a}_{i+2} \dots \mathbf{a}_M \mathbf{E}^{-1} \mathbf{Y}_M = \mathbf{E} \mathbf{T} \mathbf{E}^{-1} \mathbf{Y}_M \quad (6)$$

Consider the half-space layer in Fig.1 alone. The general solutions of differential equations of wave propagation and the stress field in the half-space layer are similar to Eqs.(2) and (4) respectively except that upward propagating reflection waves do not exist. The displacement-stress vector at the surface of the half-space layer can then be written as

$$\mathbf{Y}_M = \begin{Bmatrix} \mathbf{u}_M \\ \mathbf{t}_M \end{Bmatrix} = \mathbf{E} \boldsymbol{\kappa}' \mathbf{A}' \quad (7)$$

where matrix $\boldsymbol{\kappa}' = [\boldsymbol{\kappa}'_1, \boldsymbol{\kappa}'_2]^T$ in which submatrices $\boldsymbol{\kappa}'_1$ and $\boldsymbol{\kappa}'_2$ are defined by Eqs(A-1a) and (A-2a) in Appendix respectively, and $\mathbf{A}' = (A_1, B_1, C_1)^T$ is unknown coefficient vector determined from the boundary conditions at the surface of the half-space layer.

Substituting \mathbf{Y}_M in Eq.(7) into Eq.(6), Eq.(6) can be written as

$$\mathbf{Y}_i = \begin{Bmatrix} \mathbf{u}_i \\ \mathbf{t}_i \end{Bmatrix} = \begin{bmatrix} \mathbf{J} & \mathbf{0} \\ \mathbf{0} & \mathbf{J} \end{bmatrix} \begin{bmatrix} \mathbf{T}_{11} & \mathbf{T}_{12} \\ \mathbf{T}_{21} & \mathbf{T}_{22} \end{bmatrix} \begin{bmatrix} \boldsymbol{\kappa}'_1 \\ \boldsymbol{\kappa}'_2 \end{bmatrix} \mathbf{A}' \quad (8)$$

where $\mathbf{T}_{11} \sim \mathbf{T}_{22}$ are submatrices of matrix \mathbf{T} in Eq.(6). After some matrix manipulations of eliminating the unknown vector \mathbf{A}' , one can obtain the displacement vector \mathbf{u}_i in terms of the stress vector \mathbf{t}_i .

$$\mathbf{u}_i = \mathbf{J} (\mathbf{T}_{11} \boldsymbol{\kappa}'_1 + \mathbf{T}_{12} \boldsymbol{\kappa}'_2) (\mathbf{T}_{21} \boldsymbol{\kappa}'_1 + \mathbf{T}_{22} \boldsymbol{\kappa}'_2)^{-1} \mathbf{J}^{-1} \mathbf{t}_i = \mathbf{J} \mathbf{Q} \mathbf{J}^{-1} \mathbf{t}_i \quad (9)$$

$$\mathbf{t}_i = \mathbf{J} \mathbf{Q}^{-1} \mathbf{J}^{-1} \mathbf{u}_i \quad (9a)$$

If the layered medium has a rigid lower boundary, then $\mathbf{u}_M = \mathbf{0}$ in \mathbf{Y}_M of Eq.(6).

This leads to $\mathbf{Q} = \mathbf{T}_{12}\mathbf{T}_{22}^{-1}$ for Eq.(9).

Now, consider the upper domain(above level i). The derivation is similar to the derivation for lower domain (below level i) above (Eqs.4-9). But the boundary condition at is traction free for free surface.

Therefore, the displacement-stress vector at free surface can be expressed as

$$\mathbf{Y}_0 = \mathbf{E}\mathbf{a}_i^{-1} \cdots \mathbf{a}_i^{-1} \mathbf{E}^{-1} \bar{\mathbf{Y}}_i = \mathbf{E} \bar{\mathbf{T}} \mathbf{E}^{-1} \bar{\mathbf{Y}}_i \quad (10)$$

or

$$\begin{Bmatrix} \mathbf{u}_0 \\ \mathbf{t}_0 \end{Bmatrix} = \begin{bmatrix} \mathbf{J} & \mathbf{0} \\ \mathbf{0} & \mathbf{J} \end{bmatrix} \begin{bmatrix} \bar{\mathbf{T}}_{11} & \bar{\mathbf{T}}_{12} \\ \bar{\mathbf{T}}_{21} & \bar{\mathbf{T}}_{22} \end{bmatrix} \begin{bmatrix} \mathbf{J} & \mathbf{0} \\ \mathbf{0} & \mathbf{J} \end{bmatrix}^{-1} \begin{Bmatrix} \mathbf{u}_i \\ \bar{\mathbf{t}}_i \end{Bmatrix} \quad (10a)$$

Applying the boundary condition of free surface $\mathbf{t}_0 = \mathbf{0}$, one can obtain

$$\bar{\mathbf{t}}_i = -\mathbf{J} \bar{\mathbf{T}}_{22}^{-1} \bar{\mathbf{T}}_{21} \mathbf{J}^{-1} \mathbf{u}_i \quad (11)$$

$$\mathbf{u}_i = -\mathbf{J} \bar{\mathbf{T}}_{21}^{-1} \bar{\mathbf{T}}_{22} \mathbf{J}^{-1} \bar{\mathbf{t}}_i \quad (11a)$$

By comparing $\bar{\mathbf{t}}_i$ in Eq.(11) and \mathbf{t}_i in Eq.(9), one can say that $\mathbf{t}_i - \bar{\mathbf{t}}_i$ must be equal to n^{th} component of external load in Eq.(1) due to the stress continuity. This can be expressed as

$$\mathbf{t}_i - \bar{\mathbf{t}}_i = \mathbf{t}_n \quad (12)$$

where $\mathbf{t}_n = (\bar{\tau}_{rz}^n(r), \bar{\sigma}_{zz}^n(r), \bar{\tau}_{\theta z}^n(r))^T$ in Eq.(1)

As shown in Fig.1(b), the external loadings are assumed to be triangularly distributed. Thus, the loading distribution in r-direction can be expressed as follow;

$$\bar{\tau}_{rz}^n = h(r)p, \bar{\sigma}_{zz}^n = h(r)q, \text{ and } \bar{\tau}_{\theta z}^n = h(r)s \quad (13)$$

where

$$h(r) = \begin{cases} 1 + \frac{r-r_0}{\varepsilon} & \text{if } r_0 - \varepsilon \leq r \leq r_0 \\ 1 - \frac{r-r_0}{\varepsilon} & \text{if } r_0 \leq r \leq r_0 + \varepsilon \\ 0 & \text{otherwise} \end{cases} \quad (13a)$$

, $r_0 = \frac{r_1 + r_2}{2}$, p , q and s are intensities of these kinds of distributed loadings. The technique developed by Liou [9, 11] is employed to decompose the loadings in Eqs.(13). And after some mathematical manipulations as shown in Liou's work[9], one can obtain the following equation.

$$\bar{\tau}_n = \begin{bmatrix} \bar{\tau}_{rz}^n \\ \bar{\sigma}_{zz}^n \\ \bar{\tau}_{\theta z}^n \end{bmatrix} = \int_0^\infty \mathbf{J} \begin{bmatrix} -D_{n+1} + D_{n-1} & 0 & D_{n+1} + D_{n-1} \\ 0 & D_n & 0 \\ D_{n+1} + D_{n-1} & 0 & -D_{n+1} + D_{n-1} \end{bmatrix} \begin{bmatrix} p \\ q \\ s \end{bmatrix} dk = \int_0^\infty \mathbf{JDP} dk \quad (14)$$

where

$$\begin{aligned} D_{n+1} &= \int_{r_1}^{r_2} \frac{r}{2} J_{n+1}(kr) h(r) dr \\ D_n &= \int_{r_1}^{r_2} r J_n(kr) h(r) dr \end{aligned} \quad (14a)$$

and

$$D_{n-1} = \int_{r_1}^{r_2} \frac{r}{2} J_{n-1}(kr) h(r) dr$$

Now, one can employed Eq.(12) by substituting Eqs.(9a), (11) and (14) into Eq.(12), one can obtain

$$\mathbf{u}_i = \int_0^\infty \mathbf{J} \left[(\mathbf{T}_{21} \boldsymbol{\kappa}'_1 + \mathbf{T}_{22} \boldsymbol{\kappa}'_2) (\mathbf{T}_{11} \boldsymbol{\kappa}'_1 + \mathbf{T}_{12} \boldsymbol{\kappa}'_2)^{-1} + \bar{\mathbf{T}}_{22}^{-1} \bar{\mathbf{T}}_{21} \right]^{-1} \mathbf{DP} dk \quad (15)$$

After displacement vector $\mathbf{u}_i = (u_r, u_z, u_\theta)^T$ has been obtained, one can employ

Eqs.(9a) and (11) to calculated the stress components $\mathbf{t}_i = (\tau_{rz}, \sigma_{zz}, \tau_{\theta z})^T$ and

$\bar{\mathbf{t}}_i = (\bar{\tau}_{rz}, \bar{\sigma}_{zz}, \bar{\tau}_{\theta z})^T$ at level i for lower and upper domains in Fig.(1),

respectively .

Since the displacement vector \mathbf{u}_i and stress vectors \mathbf{t}_i and $\bar{\mathbf{t}}_i$ have been obtained , the displacement components and stress components on every horizontal plane in both domains can be calculated by using the formula similar to Eqs.(10) or (6). These formula can be derived easily.

For the stress components on the vertical cylindrical surface, one can employed the equations derived in references 9 and 11.

$$\begin{Bmatrix} \sigma_{rr} \\ \tau_{rz} \\ \tau_{r\theta} \end{Bmatrix} = \mathbf{J}_1 \mathbf{J}^{-1} \begin{Bmatrix} \tau_{rz} \\ \sigma_{zz} \\ \tau_{\theta z} \end{Bmatrix} + \mathbf{J}_2 \mathbf{J}^{-1} \begin{Bmatrix} u_r \\ u_z \\ u_\theta \end{Bmatrix} \quad (16)$$

where

$$\mathbf{J}_1 = \begin{bmatrix} 0 & -kJ_n(kr) & 0 \\ J'_n(kr) & 0 & \frac{n}{r} J_n(kr) \\ 0 & 0 & 0 \end{bmatrix} \quad (16a)$$

$$\mathbf{J}_2 = \begin{bmatrix} 2G\left(-\frac{J'_n(kr)}{r} + \frac{n^2}{r^2} J_n(kr)\right) & 0 & 2G\left(\frac{n}{r} J'_n(kr) - \frac{n}{r^2} J_n(kr)\right) \\ 0 & 0 & 0 \\ 2G\left(\frac{n}{r} J'_n(kr) - \frac{n}{r^2} J_n(kr)\right) & 0 & 2G\left(-\frac{J'_n(kr)}{r} + \left(\frac{n^2}{r^2} - \frac{k^2}{2}\right) J_n(kr)\right) \end{bmatrix} \quad (16b)$$

matrix \mathbf{J} is expressed in Eq.(3), G is shear modulus and u_r , u_z , u_θ , τ_{rz} ,

σ_{zz} and $\tau_{\theta z}$ are the displacement and stress components at horizontal plane of the

same locations where σ_{rr} , τ_{rz} and $\tau_{r\theta}$ are being calculated.

In Eq.(16b), one may observe that some elements in matrix \mathbf{J}_2 is infinite as $r \rightarrow 0$

for $n=1$. However, if the Bessel functions in the elements are expressed by polynomial functions, one can conclude that the infinite terms will be cancelled out each other in the elements. This means that there is no infinite element in matrix \mathbf{J}_2 for $r=0$.

Numerical Analysis

The solutions presented in the paper have been verified with Green function solution[10] for the case of distributed loading applied at free surface. To the cases of distributed loadings buried in layered half-space, two types of media have been chosen. One is a layer over rigid bedrock. The other is half-space. For the medium of

one layer over rigid bedrock, the nondimensional layer thickness $\bar{h} = \frac{h\omega}{2\pi Re(Cs)} = 0.5$,

in which Cs is shear wave velocity in the layer, ω is frequency, and h is thickness

of the layer. For the two types of media, the distributed loadings are buried at

nondimensional depth of $\bar{h}_i = \frac{h_i \omega}{Re(Cs)} = 0.15$, Poisson ratio is 0.33, and hysteretic damping ratio is 0.05. In order to investigate the concentration effect of the loadings, three distributed areas are selected. Referring to Fig.1(a), first case is $\bar{r}_1 = 0.125$ and

$\bar{r}_2 = 0.375$ ($\epsilon = 0.125$) in which $\bar{r}_1 = \frac{r_1 \omega}{Re(Cs)}$ and $\bar{r}_2 = \frac{r_2 \omega}{Re(Cs)}$; second case is \bar{r}_1

$= 0.2$ and $\bar{r}_2 = 0.3$ ($\epsilon = 0.05$); third case is $\bar{r}_1 = 0.225$, $\bar{r}_2 = 0.275$ ($\epsilon = 0.025$). In order to

keep the magnitude of total load equal among the three cases, the intensities are 1.0 for case 1 ($\epsilon = 0.125$), 2.5 for case 2.5 ($\epsilon = 0.05$) and 5.0 for case 3 ($\epsilon = 0.025$). Figs.2 show the real and imaginary parts of stress component σ_{zz} on the horizontal plane at $\bar{h}_i = 0.15$ for the case of one layer system with symmetric Fourier component $n=0$. The nondimensional depth $\bar{h}_i = 0.15$ means the horizontal plane is the interface where external loading is applied. In the figures, one can observe six curves representing the results at the surfaces of both upper and lower domains with $\epsilon = 0.125, 0.05$ and 0.025 respectively. From Fig.2(a), one can see that the differences between upper and lower domain surfaces only occurs at the locations where external distributed loading is applied, and the difference at $\bar{r} = 0.25$ are 5.0 for case of $\epsilon = 0.025$, 2.5 for $\epsilon = 0.05$ and 1.0 for $\epsilon = 0.125$. These 5.0, 2.5, and 1.0 are the highest intensities of distributed loads for the three cases, respectively. Referring to Fig.2(a), one can observe that stress component in the region, where external load is applied, is smaller for upper domain. Also, from Figs.2(a) and 2(b), one can observe the stress continuity at the interface of upper and lower domains. In Fig.2(b), one can also see that the imaginary part of the stress component is almost the same for $\bar{r} \geq 0.4$ for the three cases of $\epsilon = 0.125, \epsilon = 0.05$ and 0.0025 of both media. Figs.3 shows the

stress component τ_{rz} on the horizontal plane of $\bar{h}_j = 0.15$ and for the case of

half-space with symmetric Fourier component $n=1$. From the figures, one can observe the similar phenomena to that of Figs.2. One just only has to note that the stress component must multiply $\cos \theta$, if the location is not on $\theta=0$ axis. Figs.(4) show the displacement u_0 for the cases of both one layer system and half-space with $\bar{h}_j = 0.15$

and anti-symmetric Fourier component $n=0$. From Fig.4(a), one can see that the maximum displacement occurs around the location where highest intensity of loading

is applied. This phenomenon can also be observed in Figs 2.(a) and 3(a). The displacement values are getting close to each other as \bar{r} is farther away from the location where the distributed loading is applied for the three cases of $\epsilon=0.125$, 0.05, and 0.025. Also, the difference between the results for the cases of one layer system and half-space is getting apparent as \bar{r} become farther. Figs.5 show the displacement component u_z for the cases of both one-layer system and half-space with $\bar{h}_i=0.15$ and symmetric Fourier component $n=1$. From Fig.5(a), one can see that the displacement is getting closer for the case of one-layer system or half-space, if \bar{r} becomes farther. The difference among the cases of $\epsilon=0.125$, 0.05 and 0.125 only occurs at region where external loading is applied. From Figs 2-5, one also can observe that the peak values is higher as the distributed loading is more concentrated.

In order to know the effect of truncation of integrals in equations like Eq.(15), Table 1 shows the results of τ_{rz} for the case of one-layer system with $\bar{h}_i=0.15$ and $\epsilon=0.05$.

In the table, nondimensional wave number k_u is employed to replace the infinite integration limit (∞) in equations like Eq.(15). The nondimensional wave number is

nondimensionalized by shear wave velocity and frequency; i.e $k_u = \frac{kC_s}{\omega}$. Table

1 only shows the results at surface of lower domain. From the table, one can observe that the results for $k_u=2000$, 4000 and 6000 are the same up to three figures. This

means that $k_u=2000$ to replace infinite integration limit is good enough for numerical calculations. Although the numerical results for displacement components are not shown, the precision is even much better. For example, in this case, the number of significant figures is five.

Concluding remarks

After thorough numerical investigations, the presented solution is very efficient in computation. The solutions presented in the paper can be easily employed to solve the problem of elastodynamic by fundamental solution method. The advantage of the presented solution is that no singularity situation could occur in the solution process.

Acknowledgments

The financial support of this research is provided by National Science Council of Taiwan through Contract no. NSC – 101 – 2221 – E – 009 – 172
The support is appreciate.

Appendix

The matrix κ_I in Eq. (2) can be expressed as follows :

$$\kappa_I = [\kappa'_I \quad \kappa''_I] \quad (\text{A-1})$$

where

$$\kappa'_I = \begin{bmatrix} k & -v'_j & 0 \\ -v_j & k & 0 \\ 0 & 0 & 1 \end{bmatrix} \quad (\text{A-1a})$$

and

$$\kappa''_I = \begin{bmatrix} k & v'_j & 0 \\ v_j & k & 0 \\ 0 & 0 & 1 \end{bmatrix} \quad (\text{A-1b})$$

The matrix κ_2 in Eq. (4) can be expressed as follows :

$$\kappa_2 = [\kappa'_2 \quad \kappa''_2] \quad (\text{A-2})$$

where

$$\kappa'_2 = \begin{bmatrix} -2kG_j v_j & G_j(2k^2 - k_{\beta_j}^2) & 0 \\ G_j(2k^2 - k_{\beta_j}^2) & -2kG_j v'_j & 0 \\ 0 & 0 & -G_j v'_j \end{bmatrix} \quad (\text{A-2a})$$

and

$$\kappa_2'' = \begin{bmatrix} 2kG_j v_j & G_j(2k^2 - k_{\beta_j}^2) & 0 \\ G_j(2k^2 - k_{\beta_j}^2) & 2kG_j v_j' & 0 \\ 0 & 0 & G_j v_j' \end{bmatrix} \quad (\text{A-2b})$$

in which $k_{\beta_j}^2 = \frac{\omega^2}{c_{gj}^2}$, G_j is shear modulus of j^{th} layer.

The transfer matrix \mathbf{a}_j in Eq. (5) can be expressed as follows :

$$\mathbf{a}_j = \begin{bmatrix} \mathbf{a}_{11} & \mathbf{a}_{12} \\ \mathbf{a}_{21} & \mathbf{a}_{22} \end{bmatrix} \quad (\text{A-3})$$

where

$$\mathbf{a}_{11} = \begin{bmatrix} \frac{2k^2}{k_{\beta_j}^2}(CH - CH') + CH' & \frac{k}{k_{\beta_j}^2} \left((2k^2 - k_{\beta_j}^2) \frac{SH}{v_j} - 2v_j' SH' \right) & 0 \\ \frac{k}{k_{\beta_j}^2} \left(-2v_j SH + (2k^2 - k_{\beta_j}^2) \frac{SH'}{v_j'} \right) & CH - \frac{2k^2}{k_{\beta_j}^2}(CH - CH') & 0 \\ 0 & 0 & CH' \end{bmatrix} \quad (\text{A-3a})$$

$$\mathbf{a}_{12} = \begin{bmatrix} \frac{1}{G_j k_{\beta_j}^2} \left(v_j' SH' - k^2 \frac{SH}{v_j} \right) & \frac{-k}{G_j k_{\beta_j}^2} (CH - CH') & 0 \\ \frac{k}{G_j k_{\beta_j}^2} (CH - CH') & \frac{1}{G_j k_{\beta_j}^2} \left(v_j SH - k^2 \frac{SH'}{v_j'} \right) & 0 \\ 0 & 0 & -\frac{SH'}{G_j v_j'} \end{bmatrix} \quad (\text{A-3b})$$

$$\mathbf{a}_{21} = \begin{bmatrix} G_j \left(\frac{-4k^2}{k_{\beta_j}^2} v_j SH + \frac{(2k^2 - k_{\beta_j}^2)^2 SH'}{k_{\beta_j}^2 v_j'} \right) & \frac{-2kG_j}{k_{\beta_j}^2} (2k^2 - k_{\beta_j}^2) (CH - CH') & 0 \\ \frac{2kG_j}{k_{\beta_j}^2} (2k^2 - k_{\beta_j}^2) (CH - CH') & G_j \left(\frac{(2k^2 - k_{\beta_j}^2)^2 SH}{k_{\beta_j}^2 v_j} - \frac{4k^2}{k_{\beta_j}^2} v_j' SH' \right) & 0 \\ 0 & 0 & -G_j v_j' SH' \end{bmatrix} \quad (\text{A-3c})$$

$$\mathbf{a}_{22} = \begin{bmatrix} \frac{2k^2}{k_{\beta_j}^2}(CH - CH') + CH' & \frac{k}{k_{\beta_j}} \left(2v_j SH - (2k^2 - k_{\beta_j}^2) \frac{SH'}{v_j'} \right) & 0 \\ \frac{k}{k_{\beta_j}^2} \left(2v_j' SH' - (2k^2 - k_{\beta_j}^2) \frac{SH}{v_j} \right) & CH - \frac{2k^2}{k_{\beta_j}^2}(CH - CH') & 0 \\ 0 & 0 & CH' \end{bmatrix} \quad (\text{A-3d})$$

in which $SH = \sinh v_j d_j$, $SH' = \sinh v_j' d_j$, $CH = \cosh v_j d_j$, and $CH' = \cosh v_j' d_j$.

References

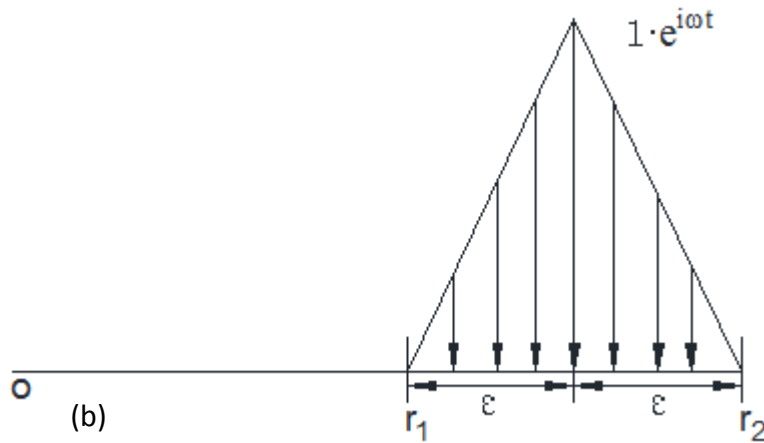
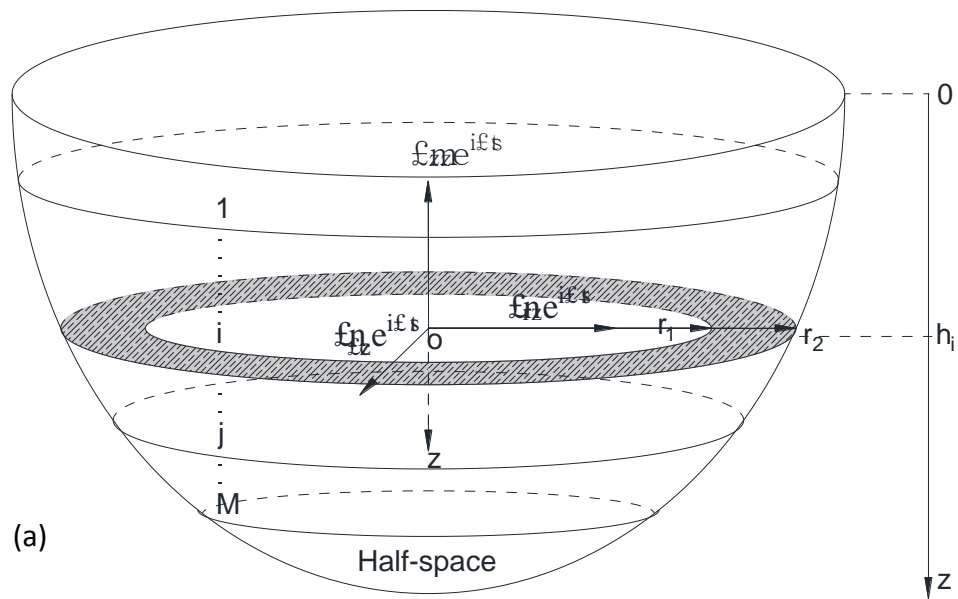
- [1] R. D. Woods, P. J. Larry, "Energy-Attenuation Relationships from Construction Vibrations," Proceedings of Vibration Problems in Geotechnical Engineering Convention, Detroit, Michigan(1985), 229-246.
- [2] X. Sheng, C. J. C. Jones, M. Petyt, "Ground vibration generated by a load moving along a railway track ", Journal of Sound and Vibration, 228(1) (1999), 129-156.
- [3] V. V. Krylov, "Vibrational impact of high-speed trains. I. Effect of track dynamics. ", Journal of the Acoustical Society of America, 100(5) (1996), 3121-3134.
- [4] Amir M. Kaynic, Christian Madshus, Peter Zackrisson, "Ground vibration from high-speed train: prediction and countermeasure." Journal of Geotechnical and Geoenvironmental Engineering , 126 (6) (2000), 0531-0573.
- [5] Anders Karlstrom, "An analytical model for ground vibrations from accelerating trains" Journal of Sound and Vibration, 293 (2006), 587-598.
- [6] R. J. Apsel, J. E. Luco, "On the Green's functions for a layered half-space, part II " Bulletin of Seismological Society of America 73 (4) (1983) 931-951.
- [7] A.V.Vostroukhov, S.N.Verichev, A.W.M. Kok , C.Esveld"Steady-state response

of a stratified half-space subjected to a horizontal arbitrary buried uniform load applied at a circular area”Soil Dynamics and Earthquake Engineering 24 (2004) 449-459.

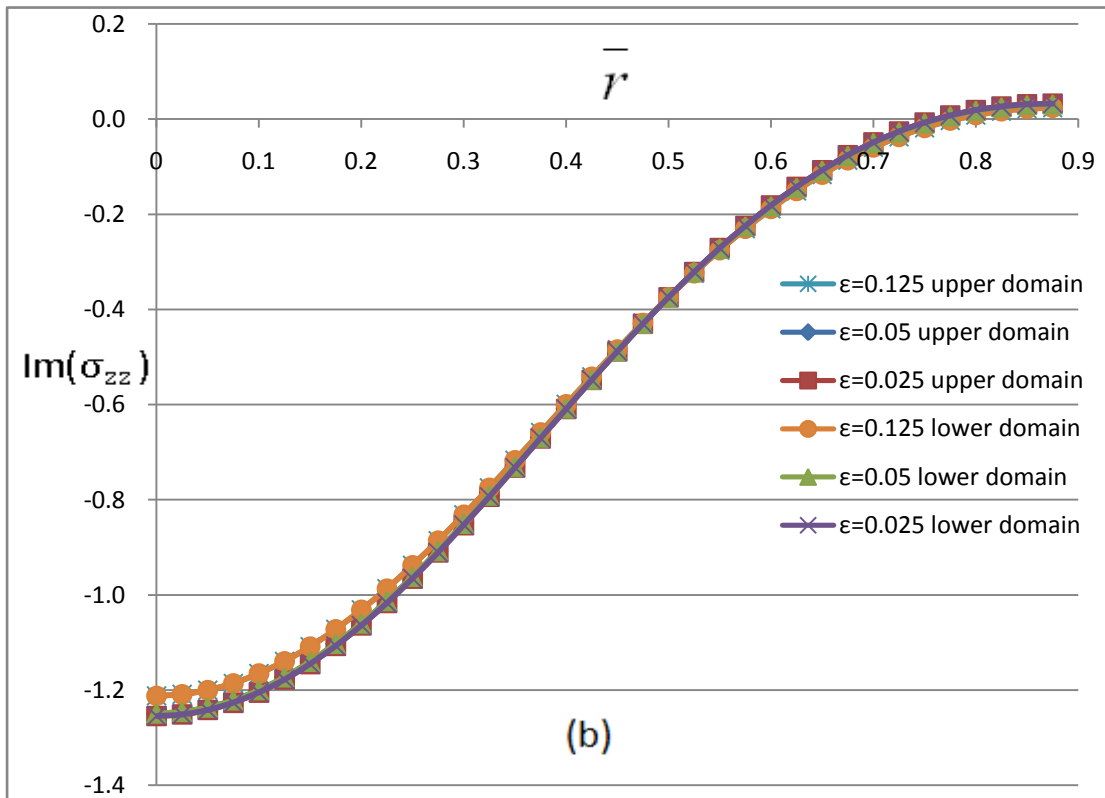
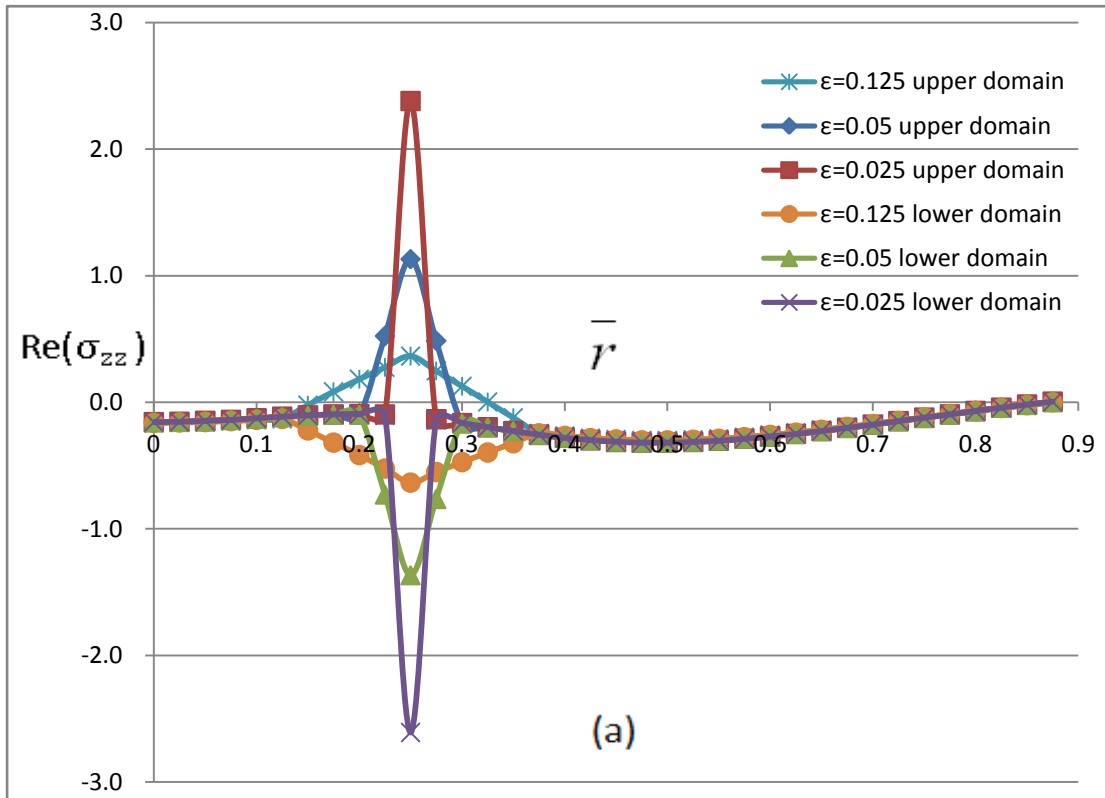
- [8]Eduardo Kausel, and Ralf Peek, “Dynamic Loads In The Interior Of a Layered Stratum: An Explicit Solution ”Bulletin of the Seismological Society of America Vol.72 , No.5, (1982), 1459-1481
- [9] G.-S. Liou, “Analytical solution for soil-structure interaction in layered media. ” J. of Earthquake Engineering. And Struct. Dynamics, 18(5), (1989) ,667-686
- [10] G.-S. Liou,“Vibrations induced by harmonic loadings applied at circular rigid plate on half-space medium.”Journal of Sound and Vibration, 323 (1-2), (2009) 257-269.
- [11] G.-S. Liou, I-L Chung. “Impedance matrices for circular foundation embedded in layered medium.”Soil Dyn Earthquake Eng, 29 (4), (2009), 677-692.

Table 1: Comparisons for different upper limits to replace infinite limit

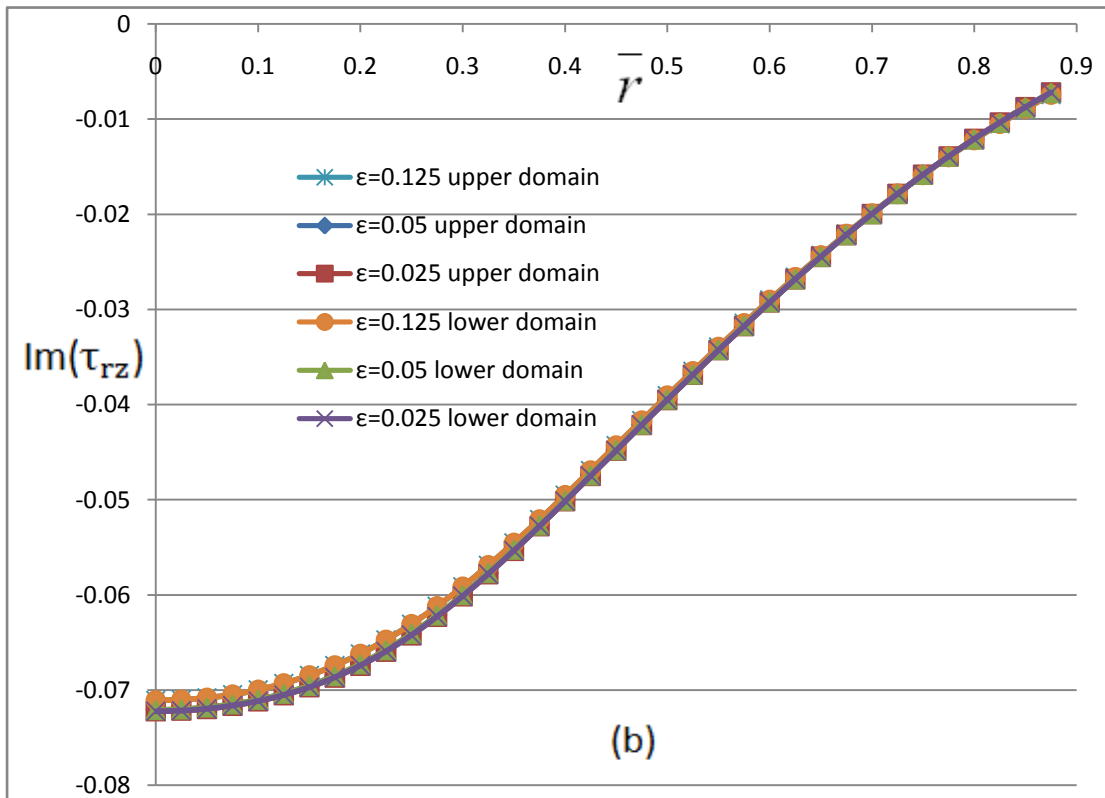
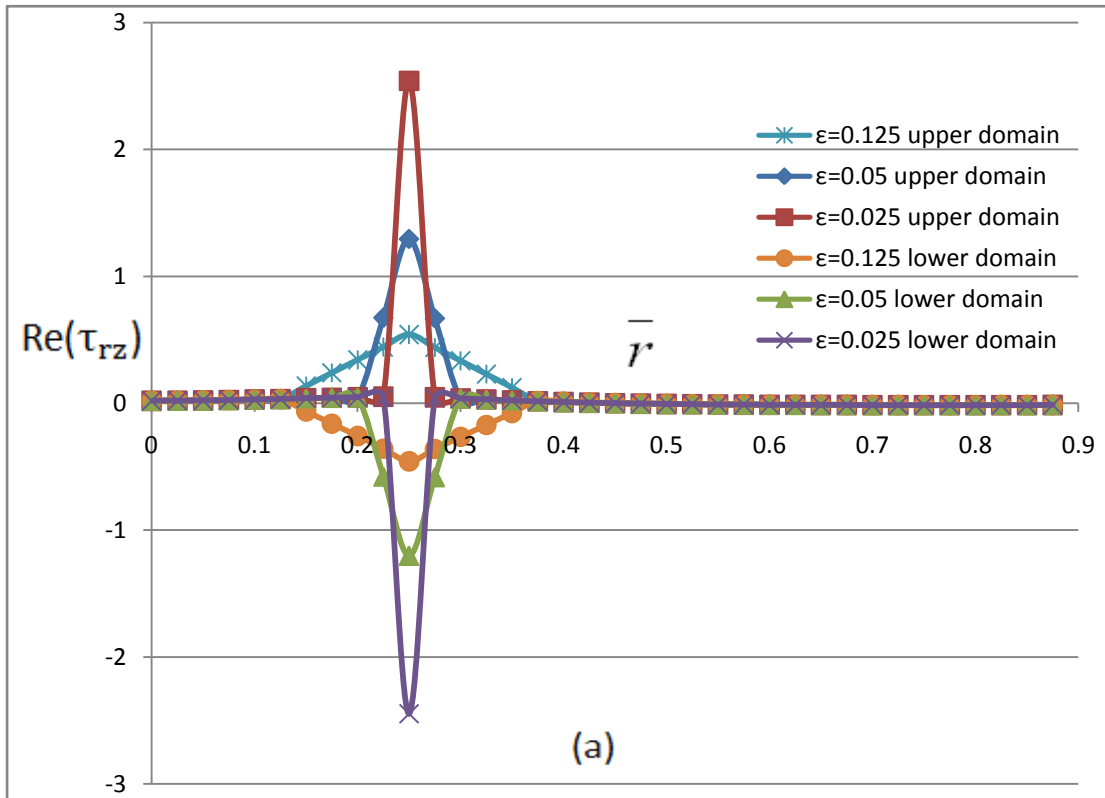
\bar{r}	Ku=2000		Ku=4000		Ku=6000	
	Re(τ_{rz})	Im(τ_{rz})	Re(τ_{rz})	Im(τ_{rz})	Re(τ_{rz})	Im(τ_{rz})
0	-8.2228E-03	-2.8991E-02	-8.0849E-03	-2.8991E-02	-8.0966E-03	-2.8991E-02
0.05	-6.9639E-03	-2.8770E-02	-6.9754E-03	-2.8770E-02	-6.9764E-03	-2.8770E-02
0.1	-3.7614E-03	-2.8099E-02	-3.7790E-03	-2.8099E-02	-3.7794E-03	-2.8099E-02
0.15	7.2696E-04	-2.6952E-02	7.2346E-04	-2.6952E-02	7.2367E-04	-2.6952E-02
0.2	6.0444E-03	-2.5293E-02	5.3113E-03	-2.5293E-02	5.0636E-03	-2.5293E-02
0.25	5.0236E-01	-2.3109E-02	5.0386E-01	-2.3109E-02	5.0436E-01	-2.3109E-02
0.3	3.8542E-03	-2.0455E-02	3.1113E-03	-2.0455E-02	2.8633E-03	-2.0455E-02
0.35	-2.6027E-03	-1.7463E-02	-2.6095E-03	-1.7463E-02	-2.6097E-03	-1.7463E-02
0.4	-7.1666E-03	-1.4301E-02	-7.1725E-03	-1.4301E-02	-7.1728E-03	-1.4301E-02
0.45	-1.0149E-02	-1.1121E-02	-1.0149E-02	-1.1121E-02	-1.0149E-02	-1.1121E-02
0.5	-1.1605E-02	-8.0392E-03	-1.1602E-02	-8.0392E-03	-1.1603E-02	-8.0392E-03
0.55	-1.2016E-02	-5.1423E-03	-1.2015E-02	-5.1423E-03	-1.2015E-02	-5.1423E-03
0.6	-1.1790E-02	-2.4965E-03	-1.1791E-02	-2.4965E-03	-1.1791E-02	-2.4965E-03
0.65	-1.1165E-02	-1.5093E-04	-1.1166E-02	-1.5093E-04	-1.1166E-02	-1.5093E-04
0.7	-1.0268E-02	1.8603E-03	-1.0267E-02	1.8603E-03	-1.0267E-02	1.8603E-03
0.75	-9.1732E-03	3.5186E-03	-9.1724E-03	3.5186E-03	-9.1725E-03	3.5186E-03
0.8	-7.9463E-03	4.8204E-03	-7.9465E-03	4.8204E-03	-7.9466E-03	4.8204E-03
0.85	-6.6482E-03	5.7760E-03	-6.6487E-03	5.7760E-03	-6.6488E-03	5.7760E-03



Figs.1: total system of layered half-space and triangular load distribution at depth h_i

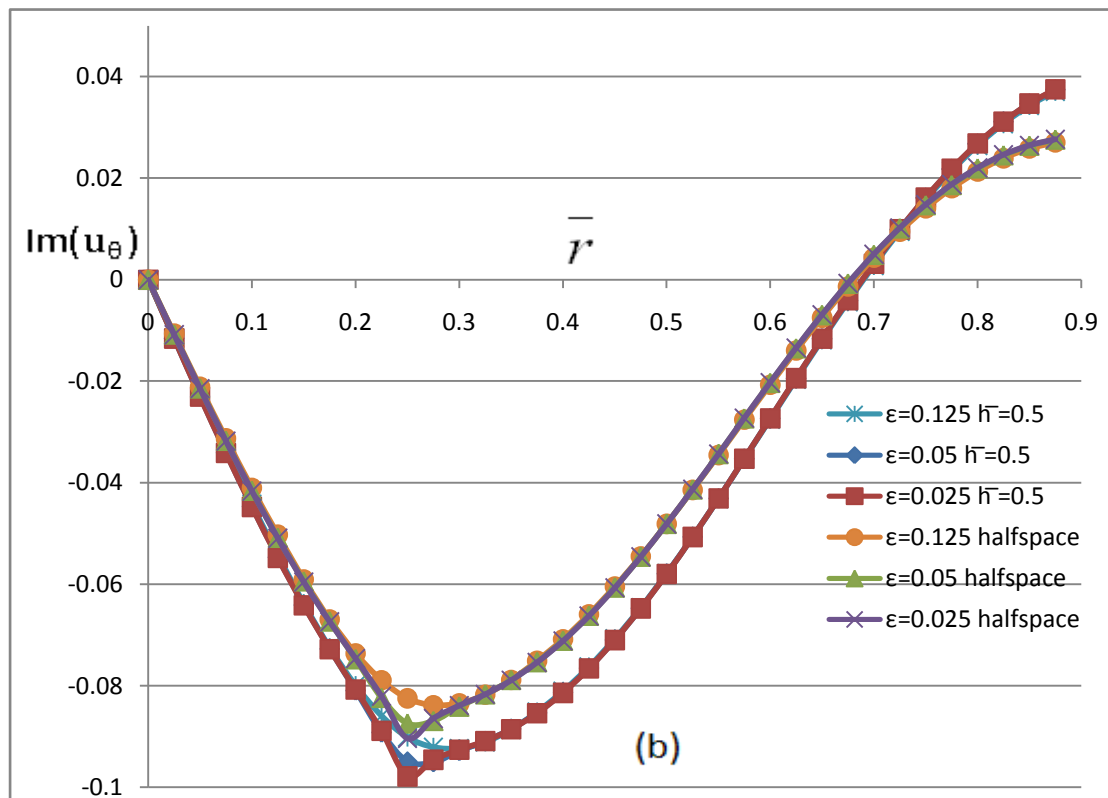
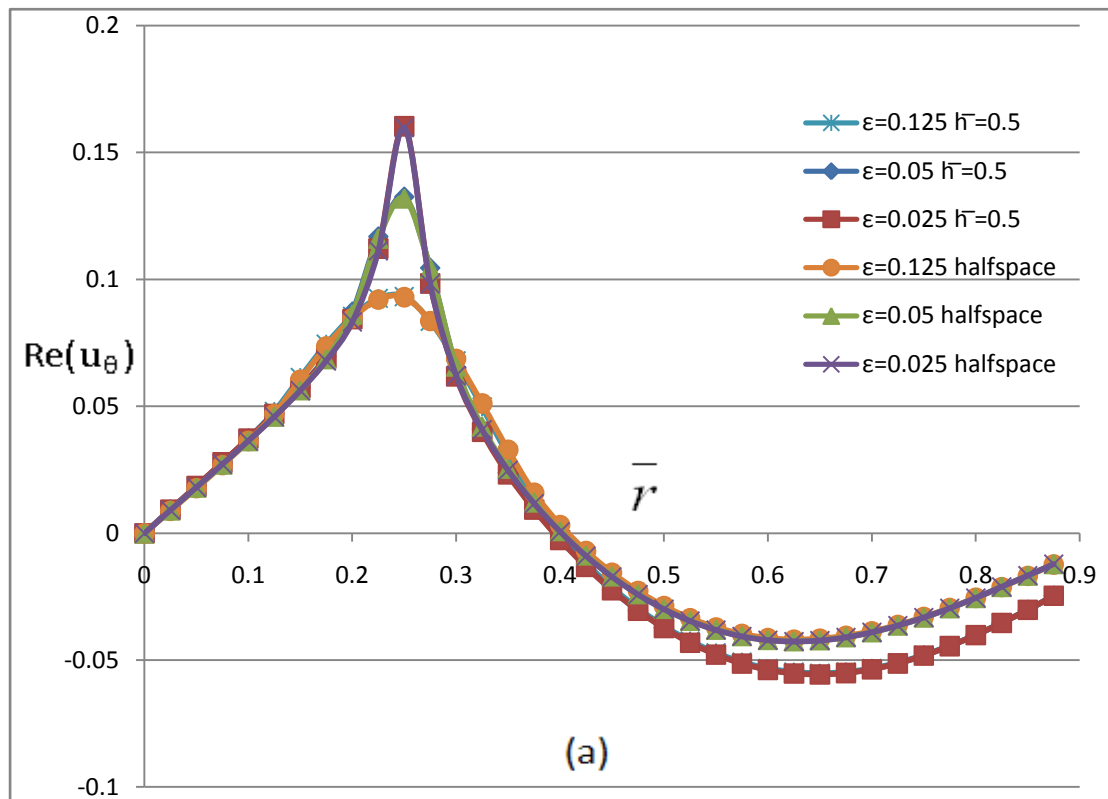


Figs.2: stress component σ_{zz} for the case of one layer over rigid bedrock, $\bar{h}_i = 0.15$ and $n=0$

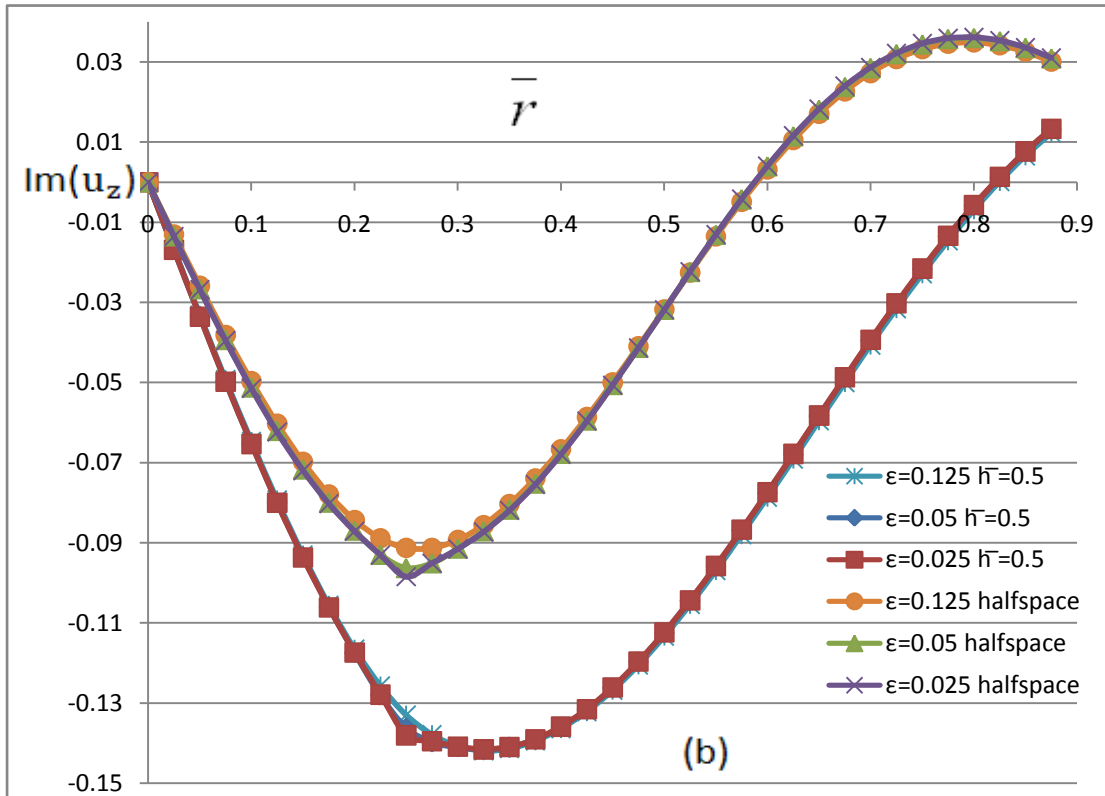
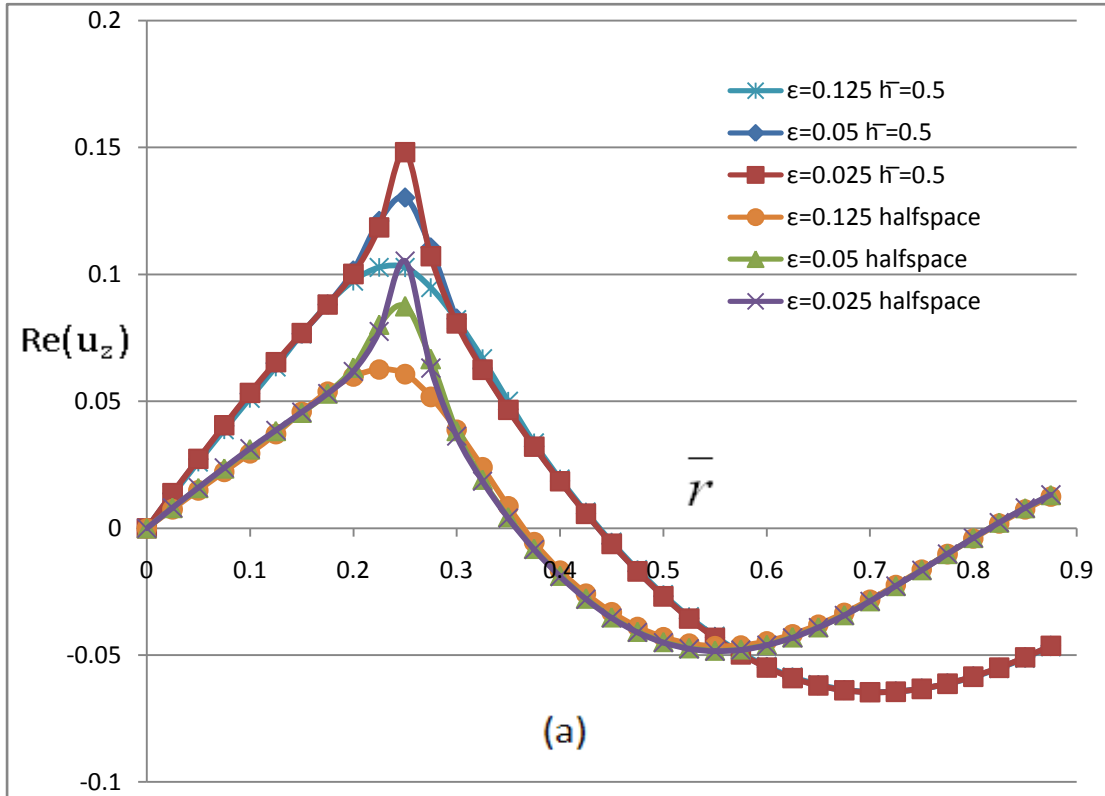


Figs.3: stress component τ_{rz} for the case of half-space, $\bar{h}_i = 0.15$

and $n=1$



Figs.4: Displacement component u_θ for the cases of one-layer system and half-space, $\bar{h}_i = 0.15$ and $n=0$



Figs.5: Displacement component u_z for the cases of one-layer system and half-space, $\bar{h}_i = 0.15$ and $n=1$

國科會補助專題研究計畫出席國際學術會議心得報告

日期：102 年 12 月 29 日

計畫編號	NSC 101-2221-E-009-172		
計畫名稱	不均勻外力作用於層狀半空間內之解析解		
出國人員姓名	劉俊秀	服務機構及職稱	國立交通大學土木工程學系(所)教授
會議時間	102 年 9 月 1 日至 102 年 9 月 4 日	會議地點	Cape Town, South Africa
會議名稱	(中文) (英文) SEMC 2013 International Conference		
發表題目	(中文) (英文) Parametric Study of Pyramid-like Tubular Structure		

一、參加會議經過

本人於九月一日到達開普敦, 當天下午報到。及聽一位 Keynote speaker 之演講。本人之 oral presentation 被安排在九月二日下午。全部論文之 oral presentation 發表的時間共三天(九月二日至九月四月), 同時有八箇平行 sessions, 故論文發表超過五百篇。九月五日後本人自行在 Cape Town 旅行數天。

二、與會心得

本次會議超過 600 多個工程師、學者參與, 其成員主要來自歐、美各國, 來自台灣只有數人參與, 因此與各國學者互動良好。參加此次會議後, 本人發現我們雖有國際知名的台北 101 大樓, 但在建築結構方面的會議卻很少參加。如此將會造成我們國內對國際建築結構的形式及其發展的概念了解甚少, 而國外之學者與工程師除了知道台北 101 大樓外, 也甚少了解國內的發展情形, 因此類似此方面的會議, 應鼓勵國內學者與工程師參加。

三、發表論文全文或摘要

Parametric Study of Pyramid-like Tubular Structure

Gin-Show Liou & Heng-Chih Kuo

Department of Civil Engineering, National Chiao Tung University, Hsin-Chu, Taiwan 30049

ABSTRACT: Framed-tube structure is a generally used structural type for tall buildings. Its basic form is closely spaced columns connected with deep spandrel beams at the periphery of building structure. This structural type is very efficient for resisting horizontal (wind) load. However, Shear lag phenomenon is the main cause to reduce the effectiveness of tubular structure. Therefore, reducing shear lag effect become a challenge to design a framed-tube structure. The paper will study the behaviors of pyramid-like tubular structure, which could effectively soothe the shear lag problem.

1 INTRODUCTION

Due to urban development and economic necessity, tall building becomes an solution for the concentration of population. As the building is getting taller, the technique to withstand the horizontal loadings induced by earthquake and wind is more demanding. To resist the horizontal loading, many structural systems are available such as large-scale bracing, core, diagrid, outrigger, framed tube structures and others as explained by Ali and Moon(2007).

Among these structure forms, framed tube structure has the advantage of arranging all the resisting component at the perimeter of the building. This makes the components more efficient to resist the overturning moment caused by horizontal loading. The concept of tubular structure was first proposed by Khan and Amin (1973). However, the disadvantage of tubular structure is the shear-lag problem. The shear lag will reduce the efficiency of the components . Therefore, bundle tubular structure is introduced as explained by Ali and Moon (2007) in order to relieve the problem of shear lag. Wang (2012) has presented the typical shear lag phenomenon in Fig. 1 for a 3x3 bundle tubular structure with some modular tubes curtailed at the heights of 400 m and 800 m. In the figure, symbol I is relative moment of inertia of cross sections of spandrel beam. However, for the higher story, Singh and Nappal (1994) have shown that negative shear lag will occur. The typical negative shear lag phenomenon is shown in Fig.2 for the 3x3 bundle tubular structure by Wang (2012). This means that the axial stress of

the interior column in the flange frame is larger than that of the exterior column. By observing Figs. 1 and 2,one can conclude that as the moment of inertia of cross section of spandrel beam (I) becomes larger, the effect of shear lag will be reduced .As the effect of shear lag is diminishing, the tubular phenomenon becomes more apparent. This can be observed in Fig. 3. In the figure, the vanishing of shear lag effect, as seen in Figs.1 and 2, will make the horizontal stiffness of the building larger. This means the lateral displacement of the building subjected to horizontal loading is reduced.

In order to mitigate the shear lag problem, a pyramid-like tubular structural form is suggested for tall buildings. The pyramid-like tubular structure is defined as the tubular structure with gradually reduced floor area through the height of floor. Since the floor area is reduced through the height, the periphery columns have to be inclined accordingly. The inclined columns can balance part of horizontal load directly. This could also mitigate the shear lag problem.

The paper will investigate the behavior of the pyramid-like tubular structure by changing the relative stiffness of spandrel beams to periphery column, and the effectiveness of the structure type for withstanding horizontal load. Also, the shear lag phenomenon for the structural type will be discussed. The analysis program SAP 2000 will be employed to model and analyze the structures. In the analysis model, only 3-D beam elements are used and rigid zone at beam-column joints is assumed.

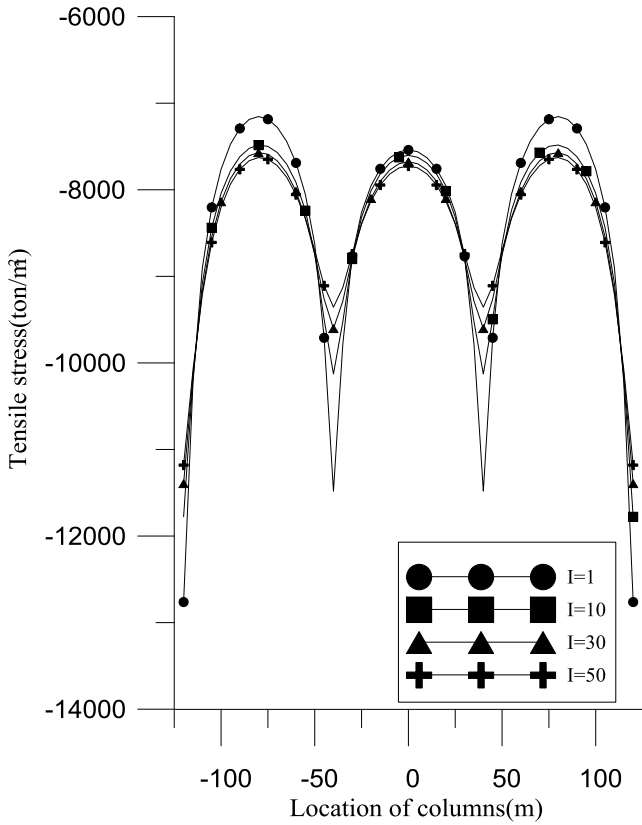


Fig. 1 Typical shear lag phenomenon for compressional flange frame at height 0m (Wang 2012)

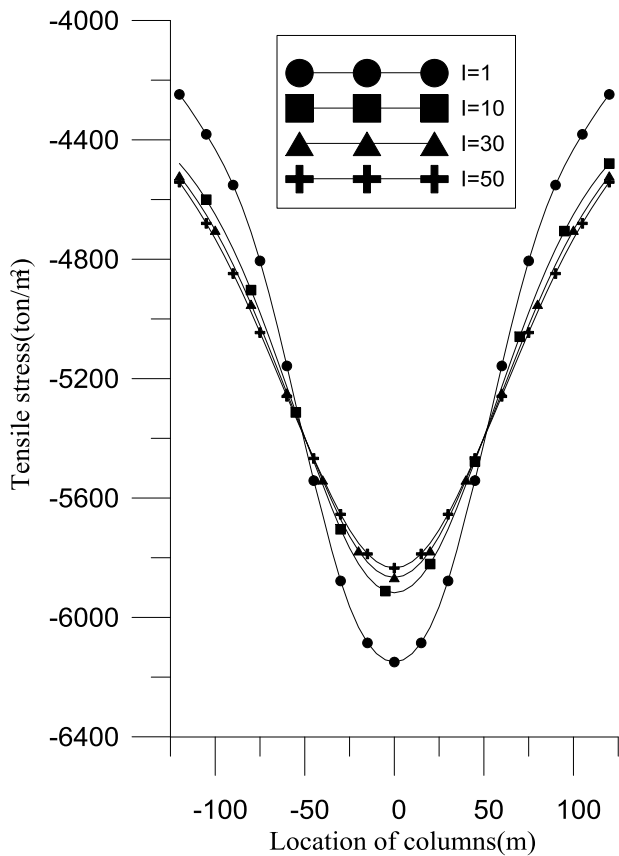


Fig. 2 Typical negative shear lag phenomenon for compressional flange frame at height 200m(Wang2012)

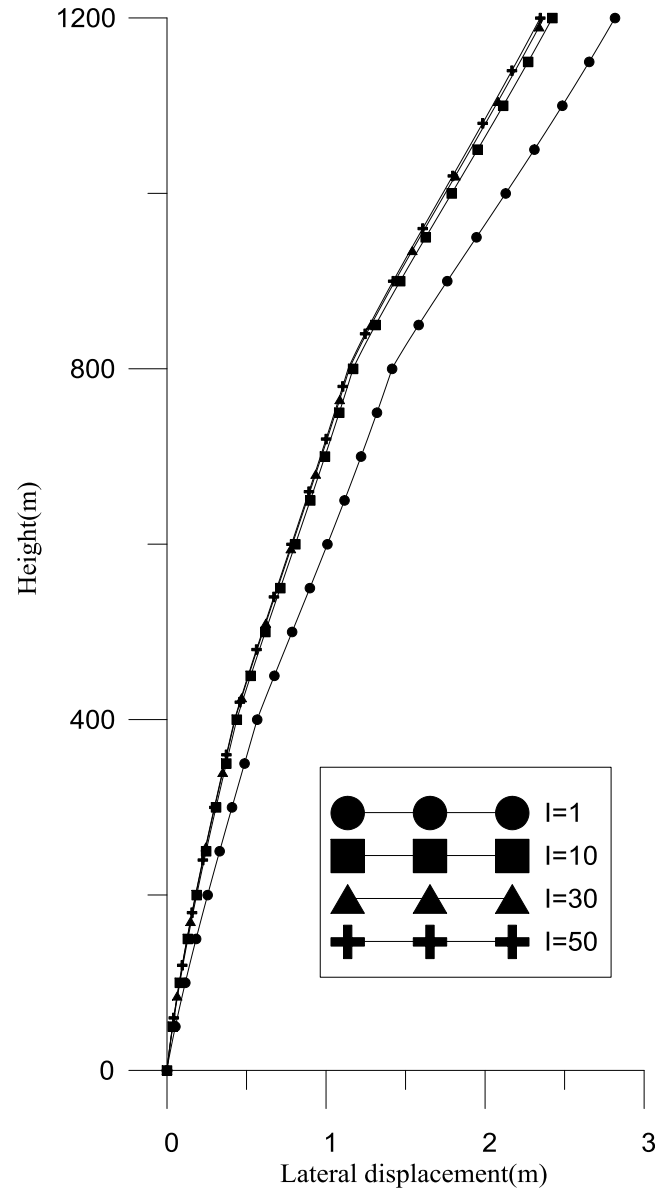


Fig. 3 Typical lateral displacement (Wang 2012)

2 NUMERICAL ANALYSIS

In order to study the behavior of pyramid-like tubular structure, the building structure shown in Fig. 4 is assumed. In the figure, the base of the structure is 240 m × 240 m and the height is 1200 m. This means the inclination of columns at periphery of the structure is 1/10 in the horizontal x and y directions. The story height is 5 m. This leads to 240 stories for the structure. The building code of Taiwan (2006) is adopted to calculate the horizontal wind load. The wind pressure on the building is shown in Fig. 5. In the figure, the wind pressure is calculated by assuming 5% damping ratio for the structure.

Computer program SAP2000 is employed to model the pyramid-like structure. In the model, only beam element is used to model columns and spandrel beams, rigid diaphragms for all the floors are assumed, and the option of rigid zones at beam-column connections is selected. The members for the four corner columns are circular tubes with 200 cm in diameter and 6 cm, 8 cm or 10 cm in thickness. The members for the other periphery columns are 100cm × 50cm rectangular tube with 6 cm, 8 cm or 10 cm in thickness. In order to keep total area of corss sections of columns constant at periphery of the structure, the spacing of the columns is 3 m for the thickness 6 cm, the spacing of the columns is 4 m for the thickness 8 cm, and the spacing of the columns is 5 m for the thickness 10 cm. Three types of member are selected for the spandrel beams. The cross sections of the three types of beams are shown in Fig. 6. Therefore, one totally has 9 cases (3 different cross sections of spandrel beams times 3 different spacing of periphery columns) to be studied. In the study, the vertical loading (gravity loading) is not taken into account. Therefore, only periphery columns and spandrel beams are modeled in Fig. 4 to resist the horizontal wind pressure shown in Fig. 5.

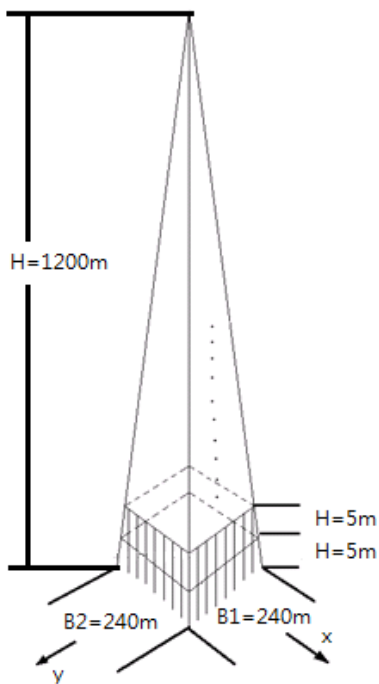


Fig. 4 Pyramid-like tubular building structure

The lateral displacement due to the wind load of Fig. 5 is shown in Fig. 7. In the figure, the symbol 3m-1 represents the case with 3 m column spacing and spandrel beam type No. 1 of Fig. 6,

and the other similar symbols (3m-2 ... etc.) represent the corresponding cases. From Fig. 7, one can observe the phenomenons as follow :
 (1) Stiffer spandrel beam will make the lateral displacement smaller. For examples, the sways for the cases 3m-3, 4m-3 and 5m-3 are smaller, while compared to the corresponding cases 3m-2, 4m-2 and 5m-2, and 3m-1, 4m-1 and 5m-1, respectively.

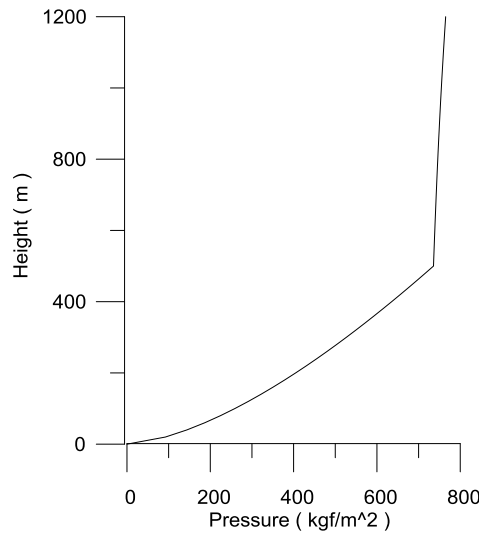


Fig.5 Design wind pressure by building code of Taiwan(2006)

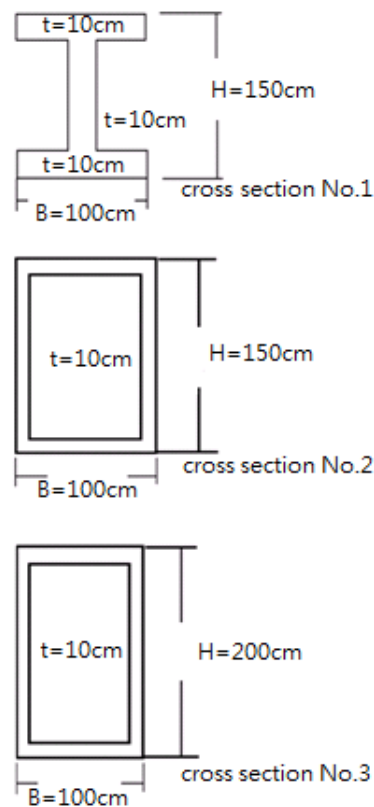


Fig. 6 Cross sections of spandrel beams

(2) If the column area is more evenly distributed around the periphery, the sway is smaller. For examples, results for the case 3m-1 is smaller than that for the cases 4m-1 and 5m-1.

(3) However, the maximum lateral displacement at top of the building structure seems entangled for the 9 cases.

Fig. 8 shows the tensile stress of the columns of flange frame at height 0 m. In the figure, one can see that the curves for shear lag phenomenon can be divided into 3 groups for the 3 types of spandrel beams shown in Fig. 6 respectively. For stronger spandrel beam, the shear lag effect is lesser. For example, the shear lag phenomenon is lightest for the strongest spandrel beam (Type No. 3 in Fig. 6). However, the effect of evenly distributed column area seems not so obvious to reduce shear lag phenomenon. This can be observed by comparing the results for cases of 3 m spacing to that for the corresponding cases of 4 m and 5 m spacings.

Figs. 9 and 10 show the tensile stress of columns at heights 200 m and 600 m respectively. From these two figures, one can observe that negative shear lag phenomenon does not occurs for all 9 cases. As a matter of fact, there is no negative shear lag observed along the height of the building, as one examines all the column stress. This could be the effect of inclination of columns.

3 CONCLUDING REMARKS

The pyramid-like structural type is suitable for super tall building. It has the advantages to effectively reduce shear lag phenomenon along periphery columns and lateral displacement along the height of building. Also, this structural type can be easily combined with other structural forms, e.g. large scale bracing and outrigger structures, to resist horizontal wind load.

4 ACKNOWLEDGMENTS

The work is partly sponsored by National Science Council of Taiwan. The support is greatly appreciated.

5 REFERENCES

- Ali, Mir M. & Kyoung, Sun Moon 2007. Structural Developments in Tall Buildings : Current Trends and Future Prospects, *Architectural Science Review* Vol 50.3 : 205-223.
- Building code of Taiwan. 2006.
- Connor, J.J. & Pouangare, C.C. 1991. Simple Model for Design of Framed-Tube Structures, *Journal of Structural Engineering*, ASCE, 117(12) : 3623-3644.
- Khan, F.R. & Amin, N.R. 1973. Analysis and design of framed tube structures for tall concrete buildings, *The Structural Engineer*, Vol.51 : 85-92.
- Singh, Y. & Nagpal, A.K. 1994. Negative Shear Lag in Framed-Tube buildings, *Journal of structural Engineering*, ASCE, 120(11) : 3105-3121.
- User's manual of SAP 2000. 2000.
- Wang, C.C. 2012. Parametric study of bundle tubular structures, *Master Thesis (In Chinese)*.

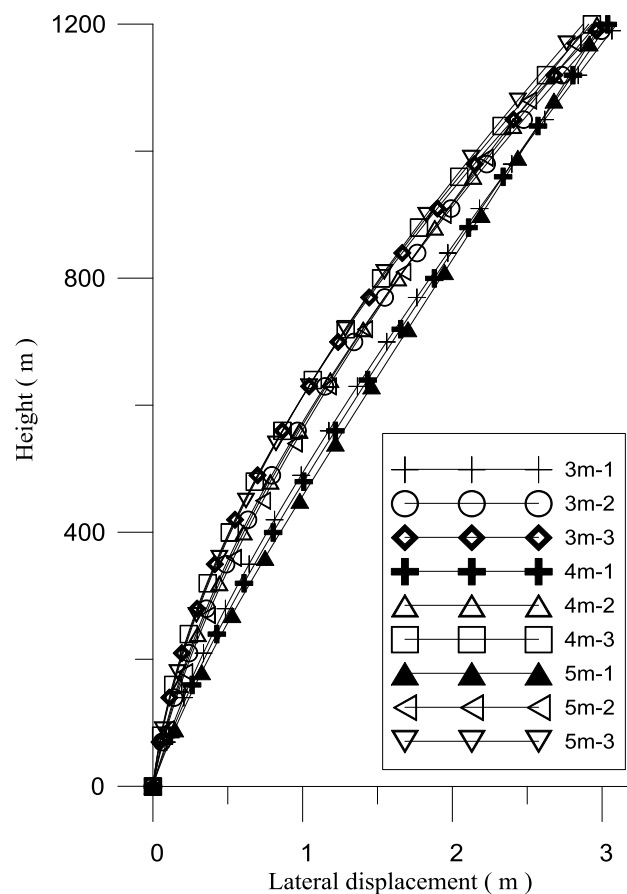


Fig. 7 Lateral displacement due to wind load

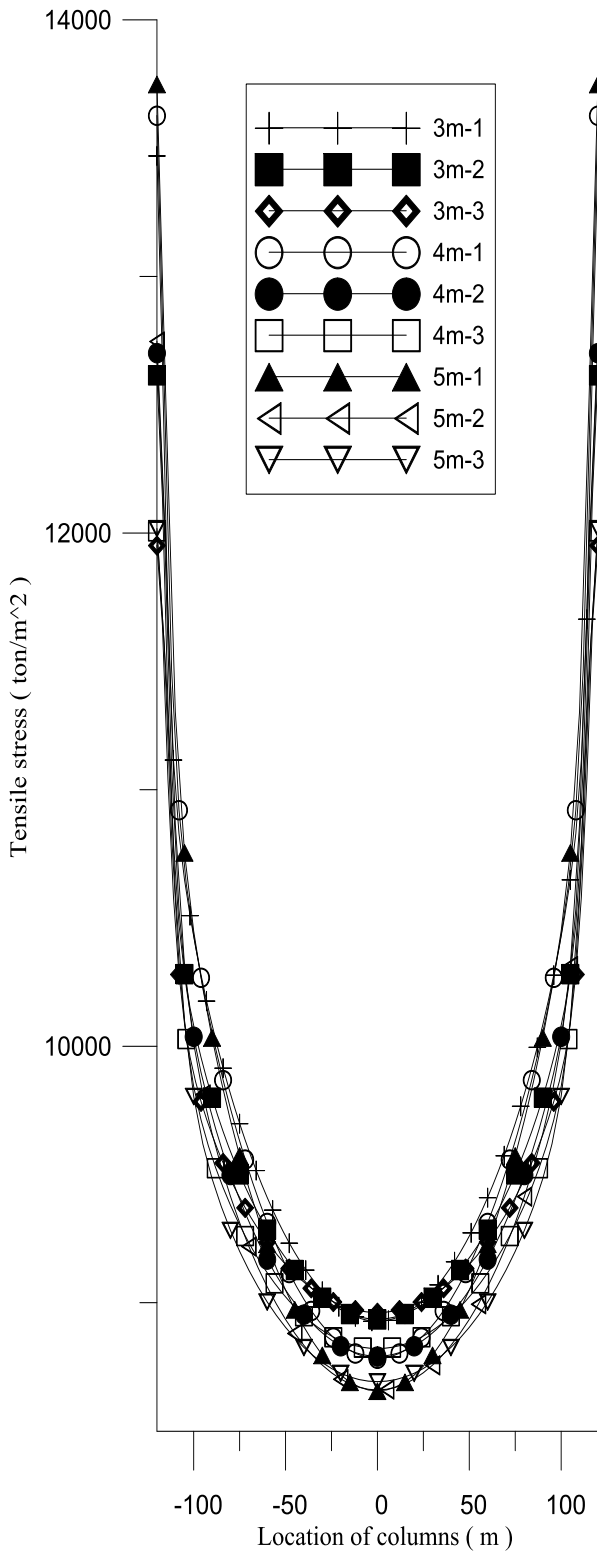


Fig. 8 Tensile stress of columns of flange frame at height 0 m(1st story)

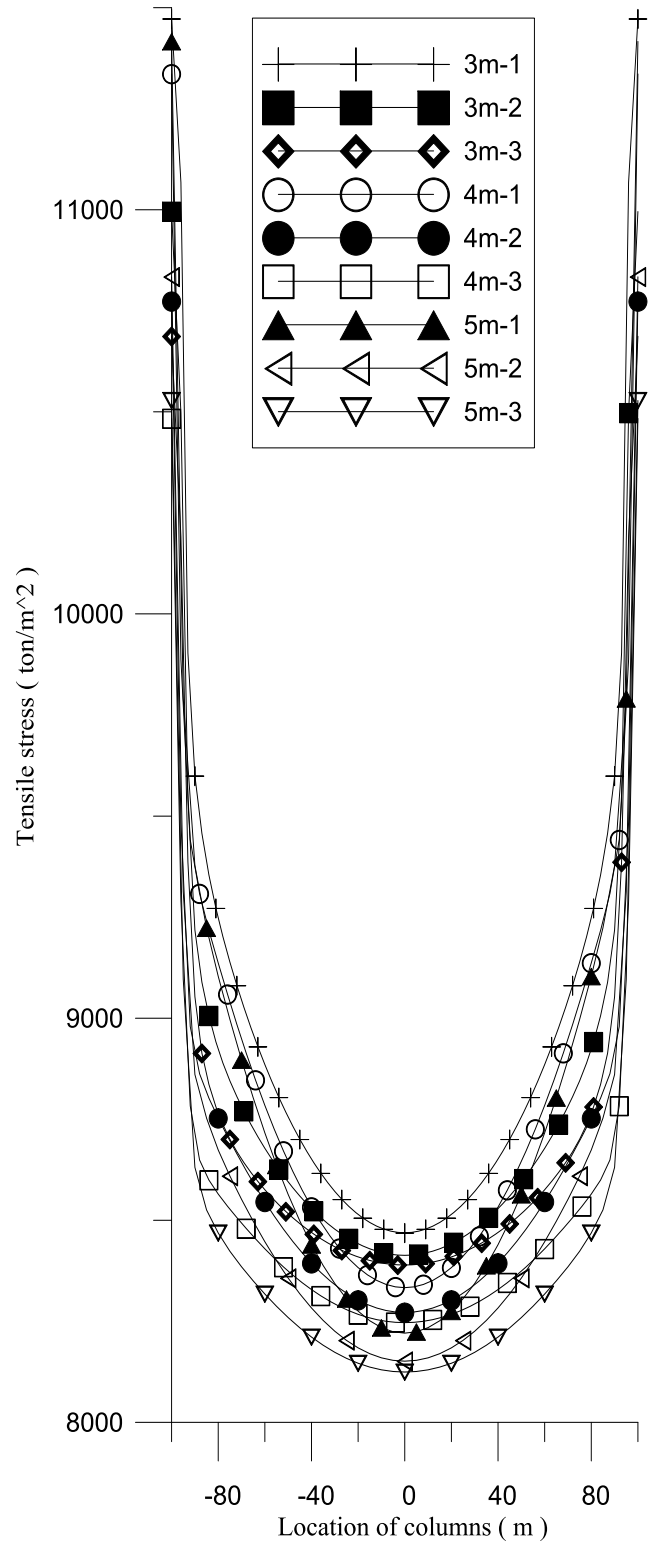


Fig. 9 Tensile stress of columns of flange frame at height 200 m

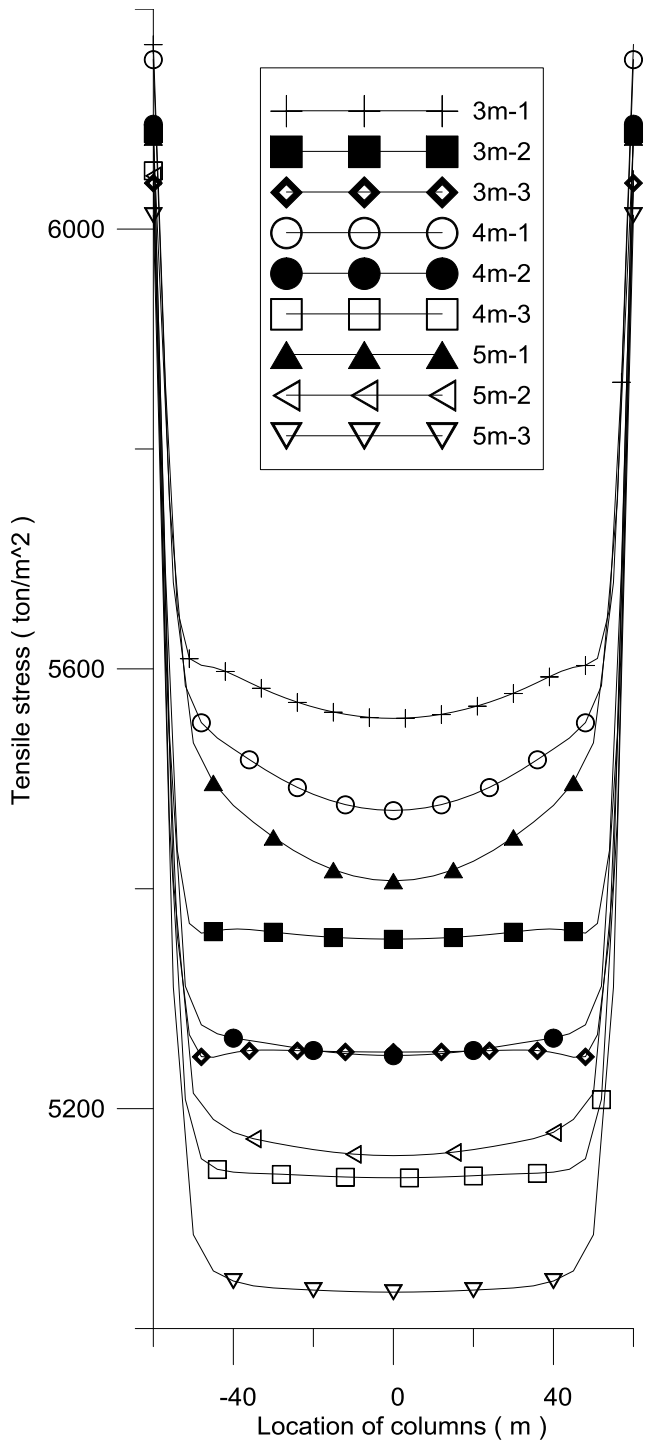


Fig. 10 Tensile stress of columns of flange frame at height 600 m

四、建議

參加國際會議不一定只參加大型會議，如小型且專門某一領域之會議，反而與國際知名的學者互動機會較多。所以有些專門領域之會議亦應鼓勵參加。

五、攜回資料名稱及內容

(1)Conference Proceedings(此為每篇文章只有二頁之長摘要(long abstract))

(2)CD 之 Conference Proceedings(此為每篇完整之文章)

六、其他

無

國科會補助計畫衍生研發成果推廣資料表

日期:2013/12/29

國科會補助計畫	計畫名稱: 不均勻外力作用於層狀半空間內之解析解
	計畫主持人: 劉俊秀
	計畫編號: 101-2221-E-009-172- 學門領域: 結構應力
無研發成果推廣資料	

101 年度專題研究計畫研究成果彙整表

計畫主持人：劉俊秀

計畫編號：101-2221-E-009-172-

計畫名稱：不均勻外力作用於層狀半空間內之解析解

成果項目		量化			單位	備註（質化說明：如數個計畫共同成果、成果列為該期刊之封面故事...等）	
		實際已達成數（被接受或已發表）	預期總達成數（含實際已達成數）	本計畫實際貢獻百分比			
國內	論文著作	期刊論文	0	0	100%	篇	
		研究報告/技術報告	0	0	100%		
		研討會論文	0	0	100%		
		專書	0	0	100%		
	專利	申請中件數	0	0	100%	件	
		已獲得件數	0	0	100%		
	技術移轉	件數	0	0	100%	件	
		權利金	0	0	100%	千元	
	參與計畫人力（本國籍）	碩士生	0	0	100%	人次	
		博士生	0	0	100%		
		博士後研究員	0	0	100%		
		專任助理	0	0	100%		
國外	論文著作	期刊論文	2	1	100%	篇	
		研究報告/技術報告	0	0	100%		
		研討會論文	1	1	100%		
		專書	0	0	100%	章/本	
	專利	申請中件數	0	0	100%	件	
		已獲得件數	0	0	100%		
	技術移轉	件數	0	0	100%	件	
		權利金	0	0	100%	千元	
	參與計畫人力（外國籍）	碩士生	2	2	100%	人次	
		博士生	1	1	100%		
		博士後研究員	0	0	100%		
		專任助理	0	0	100%		

<p style="text-align: center;">其他成果</p> <p>(無法以量化表達之成果如辦理學術活動、獲得獎項、重要國際合作、研究成果國際影響力及其他協助產業技術發展之具體效益事項等，請以文字敘述填列。)</p>	<p style="text-align: center;">無</p>
---	--------------------------------------

	成果項目	量化	名稱或內容性質簡述
科 教 處 計 畫 加 填 項 目	測驗工具(含質性與量性)	0	
	課程/模組	0	
	電腦及網路系統或工具	0	
	教材	0	
	舉辦之活動/競賽	0	
	研討會/工作坊	0	
	電子報、網站	0	
	計畫成果推廣之參與(閱聽)人數	0	

國科會補助專題研究計畫成果報告自評表

請就研究內容與原計畫相符程度、達成預期目標情況、研究成果之學術或應用價值（簡要敘述成果所代表之意義、價值、影響或進一步發展之可能性）、是否適合在學術期刊發表或申請專利、主要發現或其他有關價值等，作一綜合評估。

1. 請就研究內容與原計畫相符程度、達成預期目標情況作一綜合評估

達成目標

未達成目標（請說明，以 100 字為限）

實驗失敗

因故實驗中斷

其他原因

說明：

2. 研究成果在學術期刊發表或申請專利等情形：

論文： 已發表 未發表之文稿 撰寫中 無

專利： 已獲得 申請中 無

技轉： 已技轉 洽談中 無

其他：（以 100 字為限）

投稿 Journal of Earthquake Engineering and Structure Dynamic

3. 請依學術成就、技術創新、社會影響等方面，評估研究成果之學術或應用價值（簡要敘述成果所代表之意義、價值、影響或進一步發展之可能性）（以 500 字為限）

本研究主要突破為求得小面積內分佈載重之解析解，與 Green function 相較，本研究之解沒有奇異(singularity)值問題。